

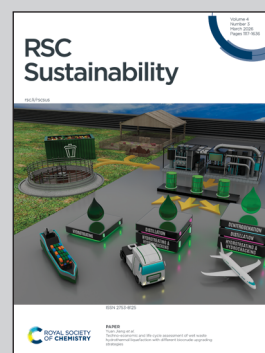
Showcasing research from Dr. Vineet Kumar's laboratory, Chemistry and Bio prospecting Division, Forest Research Institute, Dehradun, India.

EDTA-mediated crosslinking of guar gum: a sustainable platform for transdermal curcumin delivery

An efficient and sustainable green synthesis of porous and flexible EDTA-crosslinked guar galactomannan films has been accomplished that functions as an effective transdermal drug delivery system (TDDS), demonstrating non-Fickian diffusion-controlled and sustained release of curcumin from the synthesized crosslinked matrix. Such films embrace promising potential as supportive matrices for advanced organoid development in the field of biomedical applications.

Image reproduced by permission of Vineet Kumar from *RSC Sustainability*, 2026, **4**, 1376. Cover artwork created using AI.

As featured in:



See Vineet Kumar *et al.*, *RSC Sustainability*, 2026, **4**, 1376.

Cite this: *RSC Sustainability*, 2026, 4, 1376

EDTA-mediated crosslinking of guar gum: a sustainable platform for transdermal curcumin delivery

Jyoti Rajput,^{†ab} Vineet Kumar,^{id} ^{†*a} Kalpana Chauhan,^b Dhruv Kumar,^c Garima Singh^d and Ashish Mathur^{id}^d

The crosslinking of carbohydrate polymers is advantageous for specific applications in food, textiles, biomedical fields, pharmaceuticals, etc. In the present study, guar galactomannan is crosslinked with ethylenediaminetetraacetic acid (EDTA), which is a green, competent, economic, and efficient crosslinker, under aqueous conditions at ambient temperature to incorporate all carbons of the reactants into the crosslinked product. Intriguingly, EDTA acted as an autocatalyst under mild acidic conditions, resulting in water as the side product. The reaction parameters were optimized by varying the concentration of EDTA (0.25, 0.5, 0.75, and 1 g), temperature (55 ± 1 °C, 120 ± 1 °C, 130 ± 1 °C, and 140 ± 1 °C) and time (3, 2, and 1 min) to synthesize porous and flexible EDTA-crosslinked guar films. The mechanism of crosslinking with EDTA is proposed for the first time. A detailed analysis of the films is achieved by NMR spectroscopy, SEM-EDX analysis, FTIR spectroscopy, XRD and TGA. Furthermore, transdermal delivery of the loaded curcumin within the best optimized crosslinked film is studied. Mechanistic study of the curcumin release profile *via* the Korsmeyer–Peppas model demonstrated a non-Fickian diffusion-controlled release mechanism (DCR) with a CPDR of $49.8\% \pm 0.01\%$ in 720 min. The antibacterial, antifungal and antioxidant results indicate that the synthesized bio-compatible, crosslinked biomaterial has potential utility in controlled and sustained drug delivery apart from other biomedical applications such as TDDS and wound healing.

Received 29th April 2025
Accepted 18th December 2025

DOI: 10.1039/d5su00309a

rsc.li/rscsus

Sustainability spotlight

The present investigation provides a route to convert environmentally benign galactomannan into a useful product with biomedical applications by crosslinking with the multifunctional crosslinker EDTA. The use of an efficient and sustainable green chemistry approach was opted for in-depth study. Synthesis of EDTA-crosslinked guar films, as green formulations, *via* sustainable chemistry offers a myriad of benefits, catalyzing future investigations into the valorization of biomass into biomedical products and thereby addressing the sustainable and efficient use of natural resources. Hence, this work signifies a facile green synthesis by the strategic selection of reactants, solvents, catalysts, and energy sources compliant with green chemistry principles. This work emphasizes the following UNSDGs: zero hunger (SDG-2), industry, innovation, and infrastructure (SDG-9), responsible consumption and production (SDG-12) and climate action (SDG-13).

Introduction

Carbohydrate polymers are the most abundant renewable biomaterials in nature, and they have attracted significant research interest due to their environmental sustainability,

biodegradability and low cost. Due to the presence of diverse functional groups, they can be modified^{1–3} to impart desired functionalities, thereby overcoming the limitations of their native structures.^{2,4} One of the effective approaches for modification is crosslinking.^{5–7}

Crosslinked polysaccharides exhibit stronger mechanical and thermal properties and augmented solubility and swelling behavior,⁸ making them beneficial for tailored end-use applications, including biofilms for controlled drug delivery. Among polysaccharides, galactomannans have been extensively utilized for crosslinking. Interestingly, guar gum (GG) is a special galactomannan that displays an extensive array of novel and commercially valuable properties.

^aChemistry and Bioprospecting Division, Forest Research Institute, Dehradun, Uttarakhand, India. E-mail: drvineet@gmail.com

^bApplied Sciences and Humanities, School of Engineering & Technology, Central University of Haryana, Mahendergarh 123031, India

^cSchool of Health Sciences, University of Petroleum and Energy Studies, Dehradun, Uttarakhand, India

^dSchool of Allied Sciences, University of Petroleum and Energy Studies, Dehradun, Uttarakhand, India

[†] Co-first authors (authors contributed equally to this work).



Approximately 80% of guar galactomannan is produced in India, making it a highly economical and abundantly available industrial polysaccharide. After crosslinking, the biomaterial is very useful for the development of new and effective transdermal drug delivery systems (TDDS)⁹ due to greater affinity and compatibility for drugs. In the present investigation, guar gum is chosen as the polysaccharide to prepare a crosslinked matrix for TDDS due to its mucoadhesive nature, bioabsorption and low antigenicity. TDDS is one of the efficient strategies that delivers drugs at a controlled dosage through the periphery of the skin. This type of delivery system renders the key advantage of steady, non-invasive dosing while avoiding first-pass hepatic metabolism and gastrointestinal irritation.⁵⁰ Their clinical reach has broadened from conventional patches to microneedle arrays and stimuli-responsive polymer films that deliver both small molecules and biologics.^{10,52} Thus, the crosslinked polysaccharides facilitate transdermal drug delivery by providing a controlled rate of drug delivery at the targeted site and exhibit wound healing tendency *via* absorbing wound exudates and biological fluids.¹¹ Films developed from polysaccharides such as sodium alginate, carrageenan and carboxymethyl cellulose are known to exhibit physico-chemical characteristics, which are not desirable for drug delivery applications below 1% (w/v) concentration.¹² However, crosslinked guar galactomannan was found to excel in this aspect of film-forming tendency at the lowest possible concentration for favourable casting over a Petri plate. The crosslinking of carbohydrate polymers *via* a variety of synthetic, carcinogenic, expensive and non-environmentally friendly crosslinking agents such as formaldehyde,¹³ epichlorohydrin,¹⁴ toluene diisocyanate¹⁵ and glutaraldehyde¹⁶ have been previously reported. However, during the last decade, green crosslinking agents such as carboxylic acids (like citric acid, malonic acid, tannic acid, *etc.*) have gained attention due to their GRAS (generally recognized as safe) status.^{17,18} Being naturally abundant, environmentally friendly, and biodegradable,¹⁹ carboxylic acids act as platform chemicals for diversified applications.^{20,21,51}

The crosslinking potential of carboxylic acids depends upon the acid chosen for crosslinking. The number of carboxyl groups present in di-, tri-, tetra- and other-carboxylic acids influences the crosslinking reaction rate by the conversion of the available carboxyl groups into ester linkages *via* the optimization of reaction temperature and curing conditions.²² Among carboxylic acids, tetra-carboxylic acids are reported to show higher crosslinking capability than di- and tri-carboxylic acids^{23,24} due to the additional number of carboxyl groups, which makes them more facile towards activation, thereby facilitating nucleophilic attack of the polysaccharide in proximity. The higher the number of carboxylic groups, the higher is the rate of formation of the reactive cyclic anhydride intermediate, which enhances crosslinking *via* esterification under cured conditions.^{25–27}

Keeping in view the drawbacks of synthetic crosslinkers, in the present investigation, ethylenediaminetetraacetic acid (EDTA) or edetic acid has been chosen as a green crosslinker. EDTA is an underexplored yet promising green crosslinker for polysaccharide-based hydrogels. It crosslinks guar

galactomannan (GG) through a facile reaction in an aqueous medium using a green chemistry approach, resulting in the incorporation of all the carbons of EDTA in the product. The reaction demands only mild acidic conditions (pH 5) to form the ester due to the autocatalytic action of EDTA. Being a tetra-carboxylic aminopolycarboxylate, EDTA forms multiple ester linkages with hydroxyl-rich backbones, surpassing di- and tri-carboxylic acids and avoiding the steric hindrance encountered with larger polyacids, resulting in comparatively better crosslinked films. In addition to its crosslinking efficacy, EDTA is inexpensive, biodegradable, economically viable, and provides intrinsic antimicrobial and antibiofilm activity—attributes that are advantageous for wound-care TDDS.²⁸ It is a potentiating and sensitizing agent that exhibits antimicrobial potential and antibiofilm properties, for which it finds utility in transdermal wound care applications.^{29,30} Despite being such a valuable and abundantly available crosslinker, the application of EDTA as a crosslinking agent has not been widely investigated. Recent studies have employed EDTA-crosslinked chitosan to template antibacterial silver nanocomposites,⁵³ yet analogous work with galactomannan remains scarce. Earlier EDTA-guar gum formulations were developed for hydraulic-fracturing fluids at pH \approx 12 with 20 wt% crosslinker, conditions that diminish the guar viscosity and preclude biomedical application.⁵⁴ Thus, a systematic investigation of EDTA-crosslinked guar gum films synthesized under skin-compatible, green conditions is still lacking. Addressing this gap could merge the sustainability of EDTA chemistry with the favorable rheology of galactomannan to advance next-generation TDDS. With this milieu, the synthesis of an EDTA-crosslinked guar gum films (EGG) matrix, followed by the sustained release of curcumin, was studied *via* the EGG matrix. The study further discusses the reaction mechanism of GG crosslinking with EDTA. To date, only the reaction mechanism of crosslinking with di- and tri-carboxylic acids has been reported. It is observed that EGG holds the potential to absorb wound exudates due to its controlled swelling rate and demonstrates a sustained curcumin transdermal release profile. The EGG film has been characterized by FTIR, NMR, SEM, XRD and TGA. Such crosslinked films encompass chemically stable covalent bonds, providing robust and tunable mechanical properties. Furthermore, they can be engineered for diverse practical biomedical applications, such as wound dressings or localized therapy that organoids cannot provide directly. Hence, the crosslinked films fabricated in our study exhibit promising potential as supportive matrices for organoid development, which is an advanced and evolving tool in biomedical research.⁴⁹ The green reaction is useful for its utility as TDDS.

Results and discussions

For crosslinking GG, EDTA is chosen as an appropriate crosslinking agent as it is a *tetra*-carboxylic acid containing four carboxyl groups, which can provide more reactive sites for esterification. Upon crosslinking with EDTA, no harmful by-products are formed, as shown in the proposed scheme in Fig. 1. The EDTA-crosslinked guar gum matrix (EGG) was



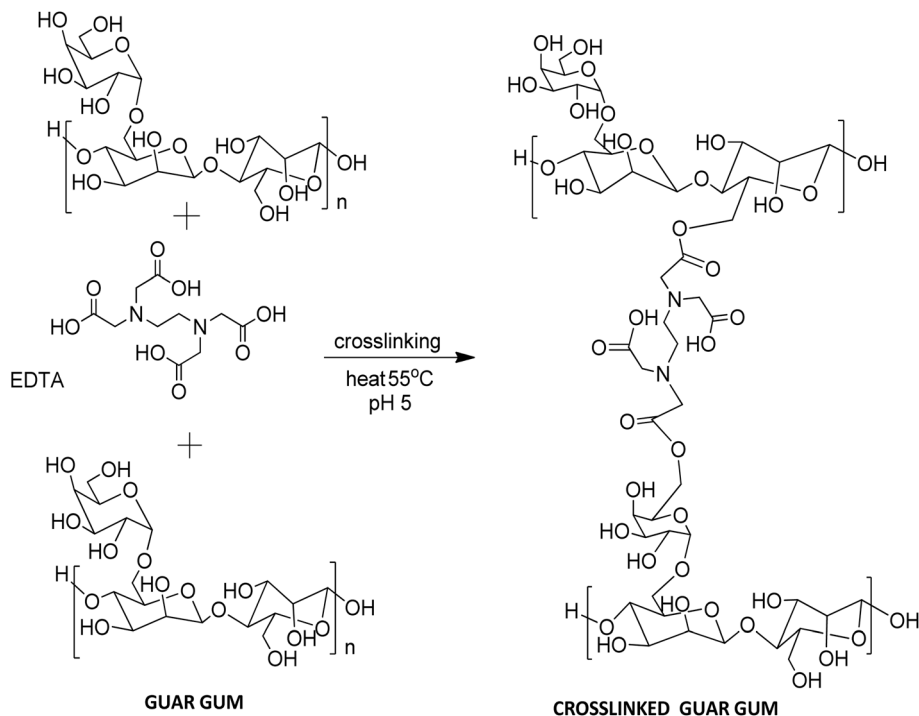


Fig. 1 Proposed scheme for the crosslinking of guar gum with EDTA at 55 °C under mild acidic conditions.

evaluated as a transdermal drug delivery system (TDDS) owing to its non-invasive nature, which offers substantial advantages over traditional administration routes. Previously, a crosslinked film of polyvinyl alcohol with 1,2,3,4-butanetetracarboxylic acid (BTCA) was used for topical wound dressings.³¹ Therefore, on using EGG as TDDS, a steady and sustained release rate of the drug is observed over an extended period, thereby reducing adverse effects and therapeutic failures of intermittent dosing. Also, the application and removal of the EGG transdermal patch on the wound surface avoids painful adhesion, subsequently leading to optimal progression of pharmacological effects. EDTA has also been approved by the FDA for the treatment of lead poisoning in adults and children. It has been prescribed by physicians for decades due to its ability to bind lead tightly, and it is more efficient than other common chelators. In dentistry, EDTA is widely used for root canal irrigation, removal of debris and rinsing of the tooth requiring treatment.

Mechanism

Crosslinking using *tetra*-carboxylic acid takes place *via* the activation of EDTA at pH 6.2. Subsequently, intra-molecular six-membered cyclic anhydride formation takes place. This is followed by a nucleophilic attack of the hydroxy group of guar gum at the cyclic anhydride, resulting in the ring opening and formation of a mono-ester. This formed monoester is then activated in the protonic environment, in which an intra-molecular cyclic anhydride is formed, which is again attacked by the hydroxy group of guar gum to produce the di-ester. EDTA undergoes effective ester linkage formation *via* intermediate cyclic anhydride formation. Therefore, this study also proposes

the plausible reaction mechanism of the crosslinking of guar galactomannan with EDTA, as shown in Fig. 2.

Degree of diesterification

Complexometric titration has been used for the quantification of the diester linkages of EDTA.³² The degree of diesterification has been calculated for cured EGG films at 120 ± 1 °C, 130 ± 1 °C and 140 ± 1 °C for 3, 2 and 1 min, respectively, using different concentrations of EDTA (0.25, 0.5, 0.75, and 1 g). As shown in Fig. 3, on increasing the concentration of EDTA from 0.25 to 1 g, the degree of diesterification increased from $0.0077 \pm (1.0 \times 10^{-4})$ to $0.022 \pm (0.4 \times 10^{-4})$ for films cured at 120 ± 1 °C for 3 min; films cured at 130 ± 1 °C for 2 min showed an increase from $0.0194 \pm (2.0 \times 10^{-4})$ to $0.030 \pm (0.2 \times 10^{-4})$, while the increase from $0.0174 \pm (0.2 \times 10^{-4})$ to $0.0295 \pm (1.5 \times 10^{-4})$ was observed for films cured at 140 ± 1 °C for 1 min. It was also observed that when films were cured at 140 ± 1 °C for time exceeding 2 min, the crosslinked guar galactomannan matrix texture turns brown signifying thermal degradation. Therefore, the curing temperature and time are optimized accordingly to avoid any adverse effects of overheating upon the physical morphology of the crosslinked films. It was observed that curing at 130 ± 1 °C for 2 min resulted in the most appropriate physical morphology of EGG film crosslinked with 0.75 g EDTA. This was further used for curcumin loading and *in vitro* studies. Similar findings have been reported in our previous work, where the degree of diesterification of crosslinked GG with malonic acid has been calculated using complexometric titration.³³ Previously, the quantification of citrate starch using complexometric titration has been reported.³⁴ Thus, our



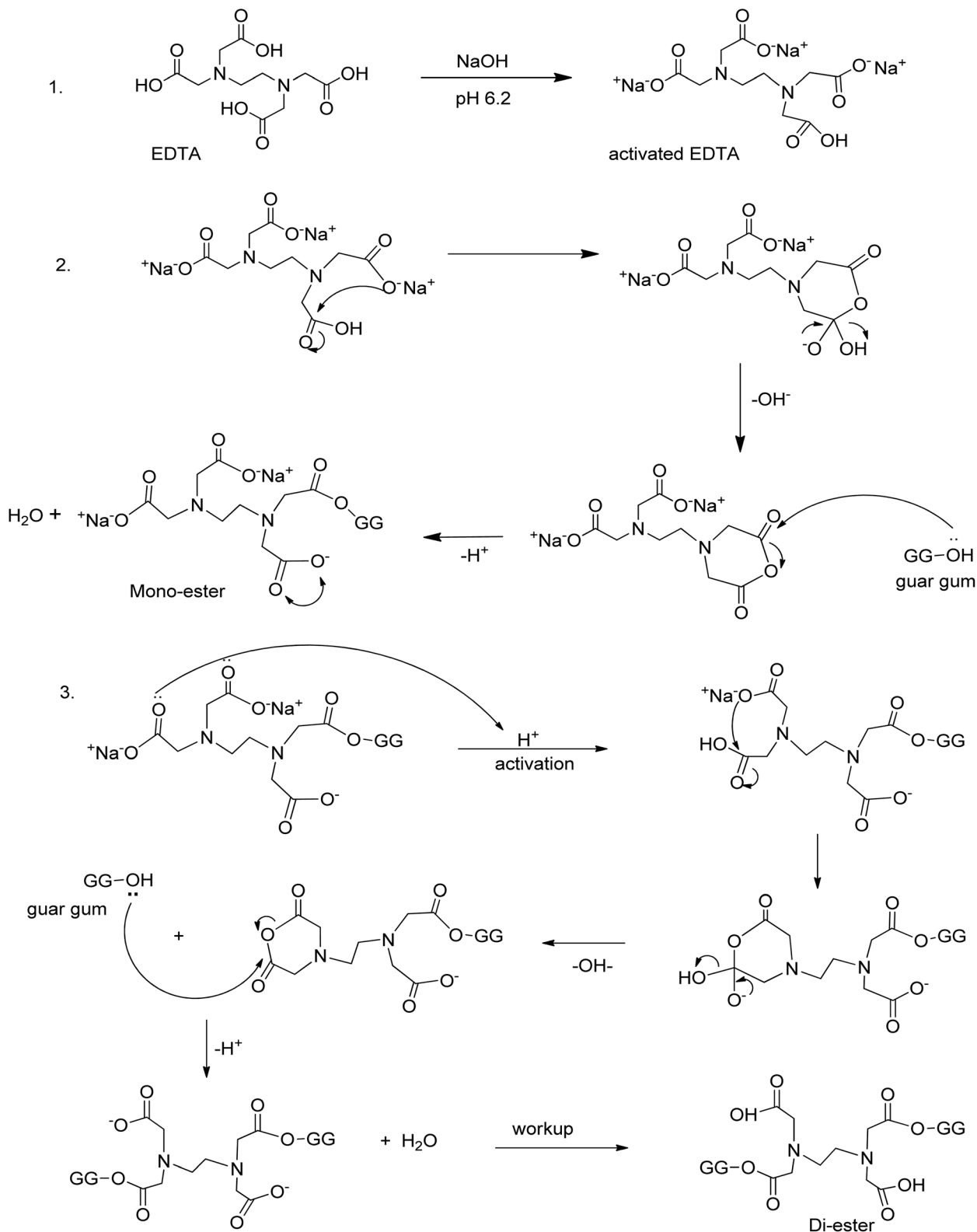


Fig. 2 Plausible reaction mechanism of the crosslinking of guar gum with EDTA.

observations and discussed results are in line with previous findings. The degree of diesterification increased as the concentration of EDTA was increased from 0.25 to 1 g.

Swelling behavior and solubility

The data depicting the solubility and swelling behavior of the EGG film are presented in Fig. 4. Due to its hydrophilic



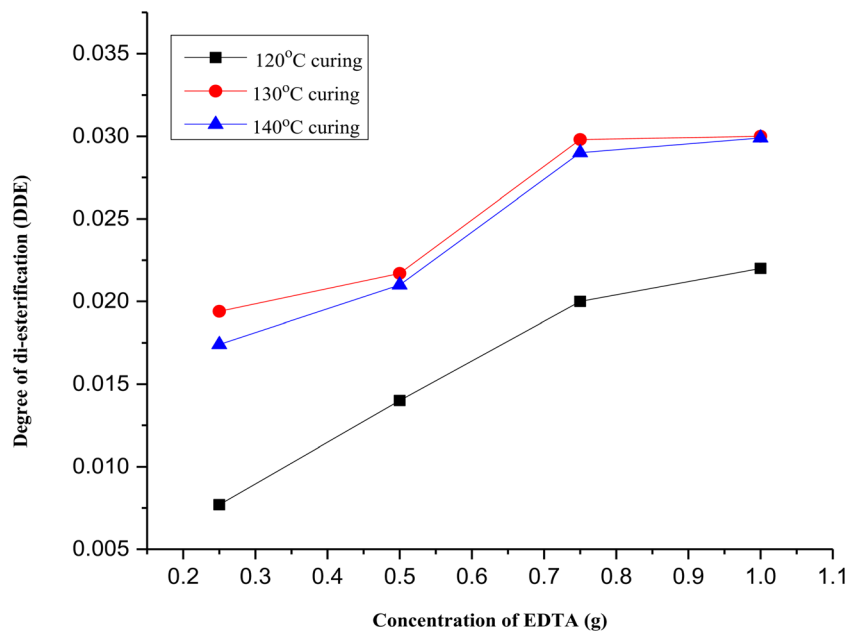


Fig. 3 Degree of diesterification vs. concentration of EDTA.

properties, GG tends to absorb water, which leads to poor mechanical integrity of the galactomannan matrix. Therefore, controlling the high swelling rate of GG is crucial for its diversified industrial applications. In the present work, it was observed that the increase in EDTA concentration from 0.25 g to 1 g led to a crosslinked matrix, resulting in a decrease in the swelling behavior from $576 \pm (0.31)\%$ to $417 \pm (0.35)\%$. With the increase in the crosslinking density, the water penetration into the GG gets regulated, thereby strengthening the GG

matrix. Dastidar & Netravali reported similar results, in which a starch-crosslinked film with malonic acid showed a decrease in swelling behavior as the malonic acid concentration was increased.²⁵ However, solubility follows the opposite trend to that of swelling behavior. As the concentration of EDTA is increased, the solubilized mass of the EGG film increases. This leads to an increment in solubility from $68 \pm (0.5)\%$ to $87 \pm (0.15)\%$. This is in agreement with the previous study of Dangi *et al.*, 2022, in which the guar galactomannan-crosslinked

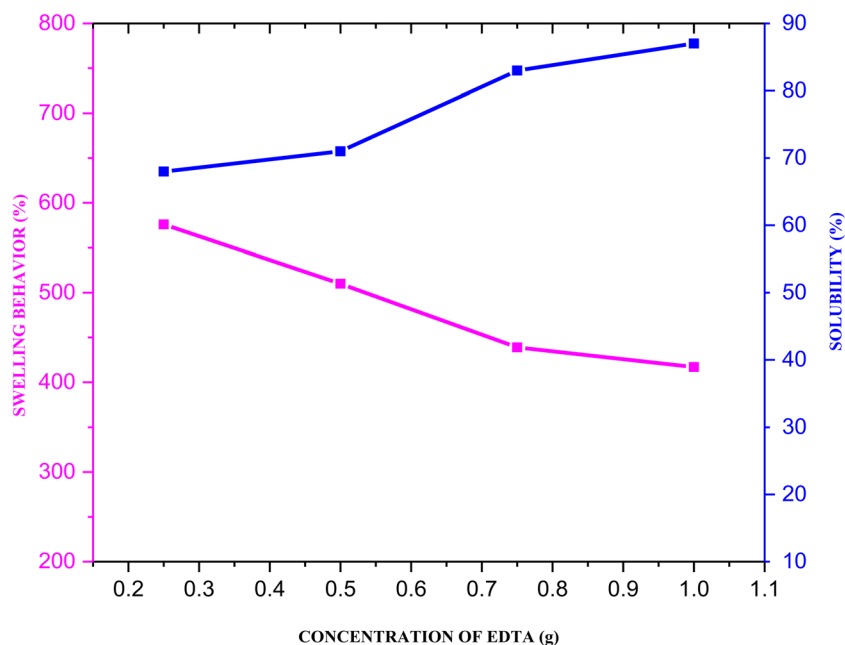


Fig. 4 Swelling behavior and solubility trend of the EGG film upon increasing the concentration of the crosslinker EDTA.



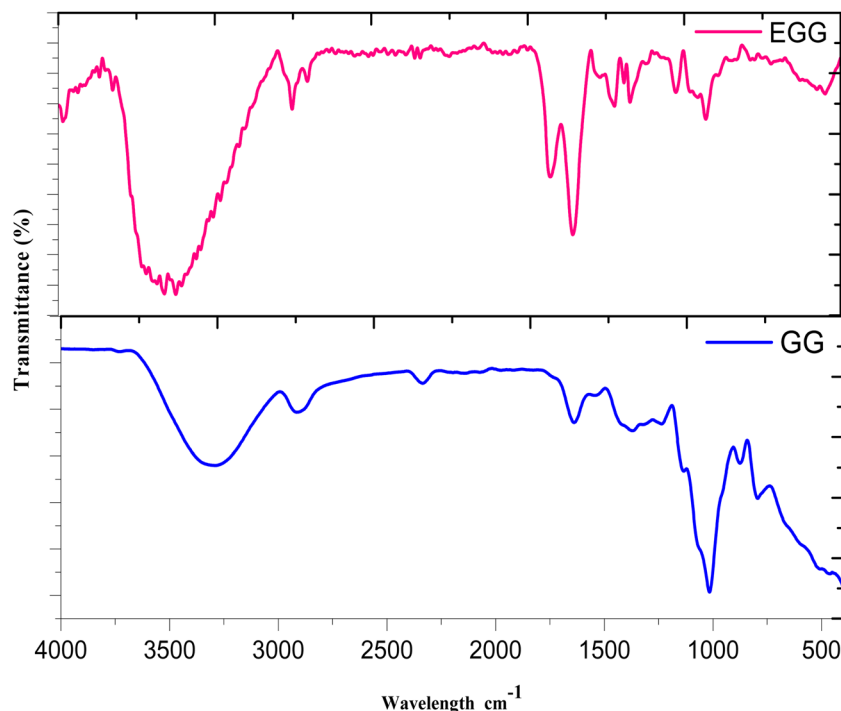


Fig. 5 FTIR spectra of GG and EGG.

hydrogel with sodium trimetaphosphate shows an increment in solubility as the crosslinker concentration is increased.³⁵

Fourier transform infrared (FTIR) study

The FTIR spectra of GG and EGG are illustrated in Fig. 5. In the GG spectra, a broad peak corresponding to O–H stretching at $\sim 3385\text{ cm}^{-1}$ becomes narrower and shifts to $\sim 3370\text{ cm}^{-1}$ due to

the involvement of hydrogen-bonded hydroxyl groups from native GG in the crosslinking process with EDTA, as shown in the EGG spectra. An additional sharp and strong peak is observed at $\sim 1738\text{ cm}^{-1}$, corresponding to the ester functional group introduced in EGG due to esterification. There is a shift observed in the characteristic C–H stretching and bending peaks of the native GG structure. In the region between 800 and

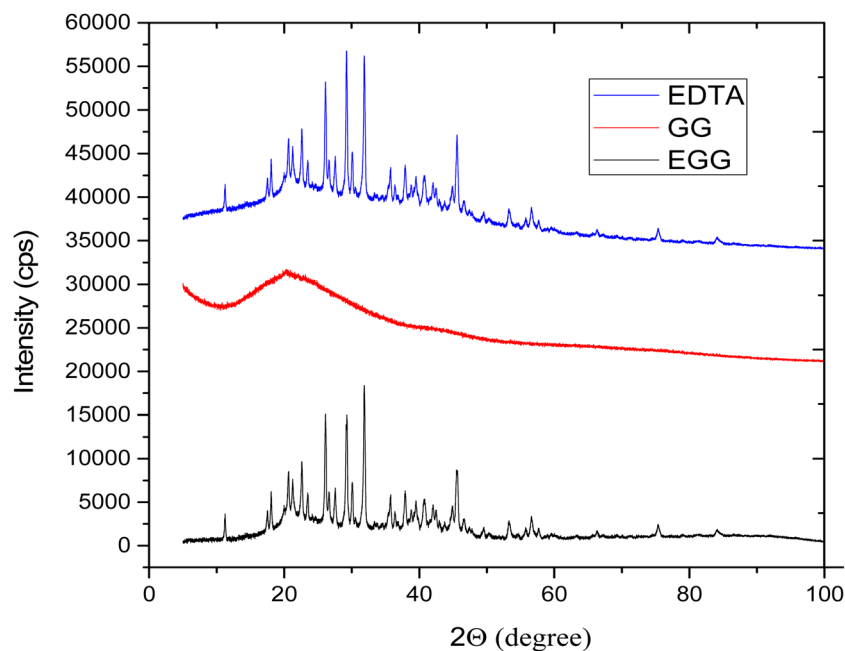


Fig. 6 XRD spectra of GG and EGG.



1300 cm^{-1} , the highly coupled C–C–O, C–O–H and C–O–C stretching peaks corresponding to the anhydroglucose units of GG and EGG appeared. An intense peak in the region around 1010 cm^{-1} corresponding to C–O–C glycosidic linkage appears in both spectra. The peak observed near $\sim 1629 \text{ cm}^{-1}$ is attributed to the bending vibration of absorbed water molecules within the GG matrix, while the peak at $\sim 1638 \text{ cm}^{-1}$ in the EGG matrix corresponds to the asymmetric stretching vibration of the carbonyl group in carboxylic acid moieties introduced through crosslinking. Thus, the FTIR spectral study validates the crosslinking done in GG's native structure.

X-ray diffraction study (XRD)

The XRD patterns of native GG and EGG are shown in Fig. 6. The native GG exhibits a slight hump-like appearance attributed to its amorphous characteristics and non-crystalline structure. Due to the higher crosslinked density of the EGG film, it has greater crystallinity than GG. Chemical crosslinking with EDTA results in a more ordered structure of the crosslinked matrix, thereby restricting the mobility of molecules and contributing to an increase in the crystalline structure of EGG. A broad hump appears at 20.53° in the GG XRD pattern. In contrast, the diffraction peaks appeared between 11° to 76° (2θ) in EGG, confirming the introduction of crystallinity in the amorphous structure of GG, thereby substantiating the FTIR results. Akar *et al.*, 2012 reported similar results when they crosslinked carboxy methyl cellulose with fumaric acid.³⁶

Scanning electron microscopy (SEM-EDX)

Scanning electron microscopy (SEM) was used to inspect the morphology of the EGG film. In the native GG film, a non-porous surface with fractured rough scales was observed, as shown in the SI. In contrast, the EGG film in Fig. 7 shows a porous, homogenous, smooth, and uniform morphology, in which fractured scales were absent. Pores of diameter in the range of 200.1–300.4 μm mainly appeared after chemical

crosslinking with EDTA. The EDX result demonstrates the elemental composition of EDTA within the EGG film. The results align with the expected outcomes, as verified by the spectroscopic methods.

TGA and DTG studies

TGA and the derivative thermograms of GG are given in the SI, while that of EGG is depicted in Fig. 8. As represented in our previous study,³⁴ the GG thermograph showed inclusive weight loss% and rate of weight loss%. Initially, 10% of weight loss was observed below 111.34°C . This loss is due to the disintegration of GG's macromolecular polymeric chains and moisture loss. With the initiation of degradation, the GG weight loss begins to occur rapidly. During this phase, 70.4% weight loss occurs (second stage) between 236°C and 634°C . The rate of weight loss% for GG also showed a two-stage mechanism in DTG. The first rate of weight loss% began before 50°C and reached a maximum rate of $0.13\%/^\circ\text{C}$ at 67°C . The second rate of weight loss% is higher than the first rate of weight loss%, with a maximum rate of $1.51\%/^\circ\text{C}$ at 300°C . At 650°C , only 12% residue was left. Fig. 8 demonstrates a three-stage weight loss of EGG initiated with 10% moisture loss after 58.72°C . The second stage weight loss of 30.1% was observed between 150.59°C and 301.3°C . In the third stage, a weight loss of 18% occurred from 312.37°C to 440°C . At 650°C , 19.5% residue was observed. DTG data of EGG also showed that the rate of weight loss% was found in three events. The first event showed a small hump due to moisture loss with a rate of weight loss% of $0.12\%/^\circ\text{C}$ at 82.04°C , while the middle event showed the maximum rate of weight loss% of $0.38\%/^\circ\text{C}$ at 272.13°C and the third event showed a rate of weight loss% of $0.31\%/^\circ\text{C}$ at 405°C . At 650°C , 19.17% of the residue is left.

Hence, from the TGA and DTG thermogram data, it can be interpreted that after crosslinking with EDTA, the thermal stability of EGG is enhanced such that the gradual degradation of GG is controlled in the respective three events of weight loss. In the case of DTG, the corresponding rate of weight loss%

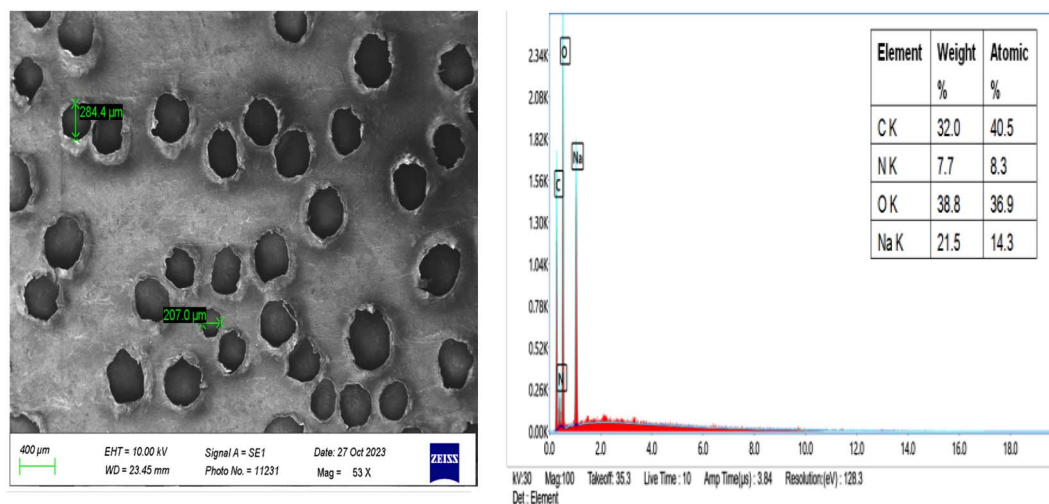


Fig. 7 SEM-EDX images of EGG.



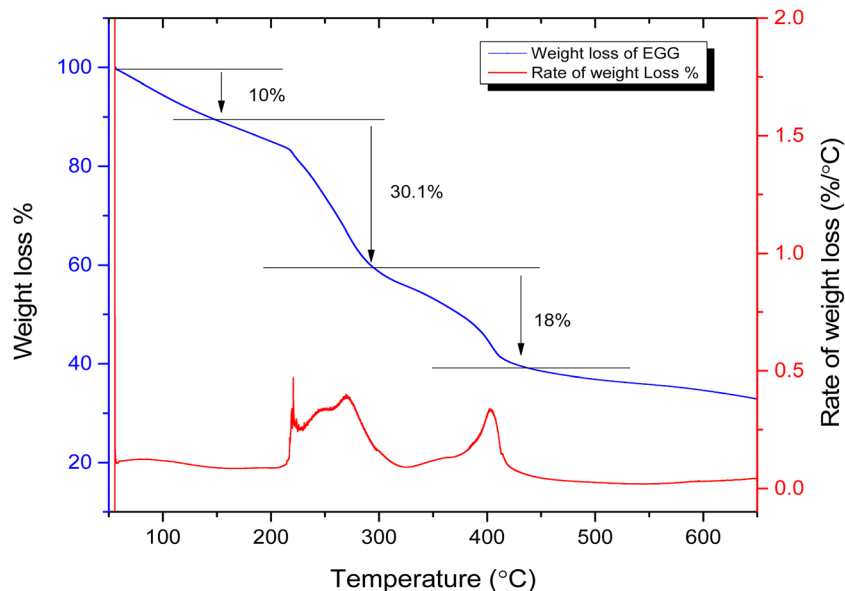


Fig. 8 TGA and DTG thermograms of EGG.

(1.51%/°C), which is the maximum at 300 °C for GG, is controlled in two events of weight loss with a lower rate of degradation. Therefore, it can be concluded that the cross-linking of guar galactomannan with EDTA is a more facile reaction.

Thickness and mechanical properties

The data on the tensile strength and elongation at break% (EAB) of GG and EGG at different concentrations of EDTA are represented in Table 1. GG has a tensile strength of $17.5 \pm (0.5)$ MPa, depicting its brittle nature. Due to its brittleness, GG has low flexibility, thereby exhibiting a poor EAB value, *i.e.*, $5.23 \pm (0.51)\%$. However, it was observed that on increasing the concentration of the crosslinker EDTA from 0.25 g to 1 g in 1% solution of guar gum, the values of EAB% considerably increased. This remarkable increment in EAB% values is due to the moisture-holding capacity of the crosslinked matrix. The enhanced flexibility on account of the increased EAB%, as depicted in Fig. 9, facilitates the transdermal release of the model drug at the targeted site. In Fig. 9, at the minimal crosslinker concentration of 0.25 g, the produced film is of poor

flexibility and easily ruptures when subjected to mechanical stress. On the contrary, as the concentration of the crosslinker is increased from 0.5 g to 1 g, the films demonstrated improved stretchability under mechanical stress. However, the tensile strength conversely decreased with the increasing concentration of EDTA, resulting in a decrease of the brittleness of native GG. This attribute facilitates effective adhesion of the film to the targeted site for drug delivery. Thus, the film inherits the desired mechanical properties for the transdermal drug delivery of curcumin.

NMR spectroscopy

The spectral data of GG have been discussed in detail in our previous study,³³ and are provided along with the spectral data of EGG in the SI. The ¹H NMR and ¹³C NMR spectra of GG and EGG are represented in Fig. 10a and b. In the ¹H NMR spectra, the signals appeared in two distinct regions, namely the anomeric and ring regions.^{37,38} In the GG spectra, the signals appearing at 5.02 ppm and 4.90 ppm depict the anomeric protons of the mannose (M1) and galactose (G1) units, respectively. Furthermore, the peaks [G2-3.82, G3-3.94, G4-4.05, G5-

Table 1 Mean values of the mechanical properties of GG and EGG

Crosslinking ratio	Thickness (mm)	Elongation at break (%)	Tensile strength (MPa)
1 : 0	$0.14 \pm (0.03)^a$	$5.23 \pm (0.51)$	$17.5 \pm (0.5)$
1 : 0.25	$0.27 \pm (0.05)$	$23.0 \pm (1.5)$	$9.03 \pm (1.5)$
1 : 0.5	$0.31 \pm (0.03)$	$24.6 \pm (2.5)$	$8.29 \pm (1.5)$
1 : 0.75	$0.32 \pm (0.05)$	$37.43 \pm (3.5)$	$7.57 \pm (0.5)$
1 : 1	$0.35 \pm (0.05)$	$44.6 \pm (1.5)$	$5.05 \pm (0.2)$
F	3.26	525.78	63.86
P	>0.05	≤0.05	≤0.05
Significant/non-significant	Non-significant	Significant	Significant

^a Values in brackets represent standard error.



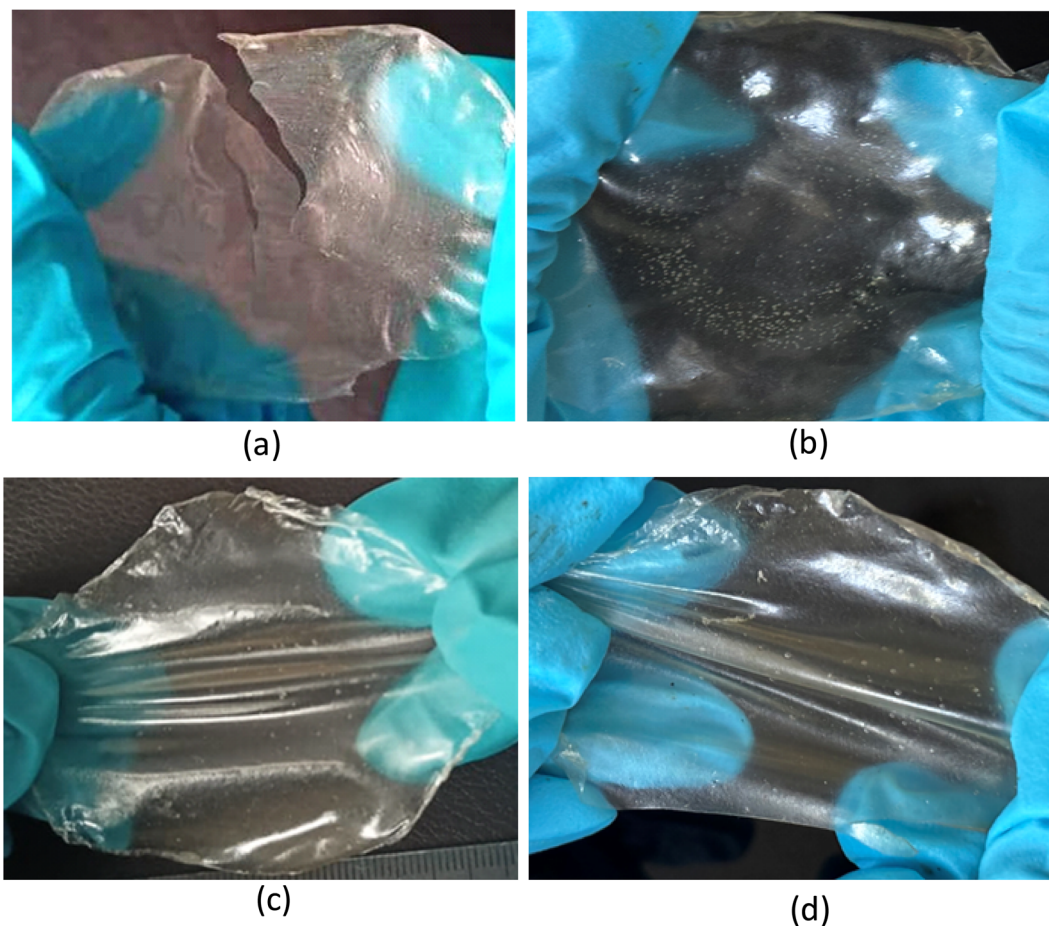


Fig. 9 Crosslinked film samples corresponding to the crosslinker EDTA concentration of (a) 0.25 g, (b) 0.5 g, (c) 0.75 g, and (d) 1 g used for thickness and mechanical testing.

3.90, G6-3.74, M2-4.13, M3-3.80, M4-3.98, M5-3.56, M6-3.75 ppm] represent the protons in the ring region. Conversely, in the ^1H NMR spectra of EGG, it is observed that after cross-linking, new peaks at carbons [C3, C7-3.48, C5, C6-3.37 and C2-3.47], corresponding to methylene protons ($-\text{CH}_2-$) of the incorporated esterified EDTA crosslinkages, appear. Furthermore, the C5 and C6 protons at 3.37 ppm appear with enhanced intensity due to the increment in the same environment protons after crosslinking, and are comparatively more shielded than the protons at the C3, C7 and C2 positions due to direct attachment with the nitrogen atom.

In the ^{13}C NMR spectra of GG, the anomeric region appeared at G1-98.63 and M1-100.18, corresponding to the galactose and mannose units, respectively. The ring region peaks appeared at positions [G2-69.82, G3-70.87, G4-70.45, G5-72.77, G6-60.96, M2-71.26, M3-73.26, M4-76.52, M5-74.99, M6-61.22]. The additional peak at C1-170.77 ppm confirms the formation of the ester linkage. Also, the peaks corresponding to carbons [C2-55.22, C3, C7-54.59 and C5, C6-51.32] ppm represent the methylene units of incorporated crosslinked EDTA ester linkages.

In the 2D-NMR analysis, many signals were overlapping. Hence, these were studied by different techniques *via* the

heteronuclear (HSQC and HMBC) correlation of chemical shifts, which is represented in the SI.^{43,45,46}

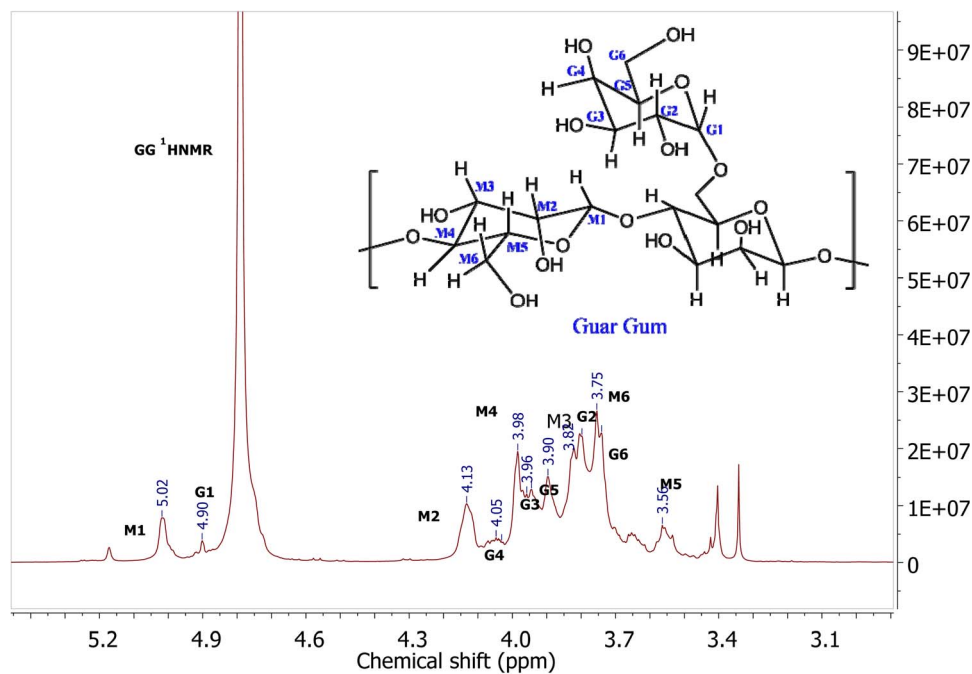
The heteronuclear coupling (HSQC) of protons and carbons shows cross-peaks at G1 (4.90, 99.26), G2 (3.82, 69.22), G3 (3.94, 69.99), G4(4.04, 70.77), G5 (3.91, 71.09), G6 (3.75, 60.94); M1 (5.02, 100.45), M2 (4.14, 70.99), M3 (3.81, 72.89), M4 (3.98, 76.82), M5 (3.57, 74.92) and M6 (3.76, 61.99) ppm in the spectra for GG. The HSQC spectra of EGG showed additional cross-peaks at C2 (3.47, 55.13), C3 (3.48, 54.58) and C5 (3.37, 51.29). The $^3J_{\text{C-H}}$ (proton-carbon) long-range coupling was studied by HMBC. The native GG showed peaks at M4-M6 (3.75, 76.91), M2-M4 (3.98, 71.05), M3-M1(3.80, 100.48), G4-G6 (4.06, 60.74), G2-G4 (3.82, 69.11) and G3-G1 (3.91, 98.43) ppm. While in EGG, an amplified cross-peak at M6-C1 (3.79, 170.11), C2-C6 (3.47, 54.66) and C7-C2 (3.48, 55.16) ppm appeared, which confirmed the ester group linkage in the GG structure.

Hence, the additional peaks in various spectra satisfactorily establish the integration of EDTA in the GG native structure.

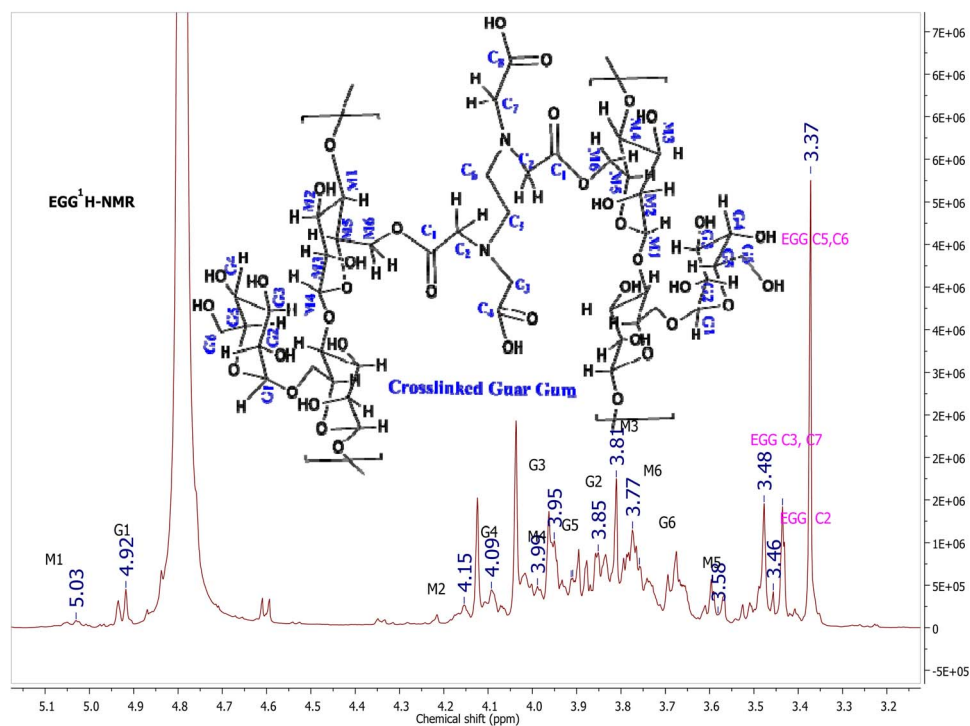
Curcumin loading and *in vitro* release study

The sustained release of curcumin from the hydrophilic matrix of EGG was facilitated in PBS at pH 7.4 *via* swelling of the crosslinked EGG matrix, through which curcumin release in





(a)



(b)

Fig. 10 (a) ^1H NMR spectrum of GG and (b) ^1H NMR spectrum of EGG.

cumulative time intervals was recorded. It was observed that the drug loading capacity (DLC) and entrapment efficiency (EE) of curcumin are $7.92 \pm (0.2)\%$ and $72.2 \pm (0.5)\%$, respectively, as shown in Table 3. In Table 2, the CPDR% of sustained release of

curcumin *via* EGG film is shown. EGG exhibits a CPDR% of $49.8 \pm (0.01)\%$ in 720 min, with a negligible increase beyond 600 min, indicating a plateau in release.



Table 2 *In vitro* CPDR% release of curcumin from the EGG matrix

Time (min)	Absorbance	CPDR%
60	0.128 ± (0.002)	10.33 ± (0.11)
120	0.154 ± (0.001)	14.26 ± (0.15)
180	0.167 ± (0.001)	19.28 ± (0.01)
240	0.196 ± (0.011)	23.63 ± (0.01)
300	0.242 ± (0.001)	28.25 ± (0.01)
360	0.269 ± (0.003)	33.3 ± (0.15)
420	0.298 ± (0.005)	37.61 ± (0.25)
480	0.314 ± (0.001)	41.28 ± (0.01)
540	0.347 ± (0.001)	45.55 ± (0.15)
600	0.382 ± (0.005)	49.57 ± (0.11)
660	0.405 ± (0.001)	49.81 ± (0.01)
720	0.404 ± (0.001)	49.8 ± (0.01)
F	4256.617	201351.8
P	≤0.05	≤0.05
Significant/non-significant	Significant	Significant

Furthermore, the *in vitro* kinetics of CPDR% of curcumin release from the loaded EGG film was studied *via* first- and second-order kinetics, whereas the mechanistic study was evaluated using the Korsmeyer–Peppas model. This model fits best because it gives the maximum value of the coefficient of determination R^2 , which comes out to be 0.9987. Applying this statistical model, the value of the release exponent 'n' comes out to be 0.76, which means that the drug release mechanism comes out to be a combined effect of erosion and diffusion. This showed that curcumin depicts a non-Fickian diffusion-controlled release (DCR) mechanism. A rate constant ' k ' = 0.37 indicates a minimal interaction between the formulated film and the loaded curcumin. This observation demonstrates that the EDTA-crosslinked guar gum film matrix exhibits a non-Fickian diffusion-controlled mechanism (DCR) of curcumin release, supporting its potential for sustained transdermal release of curcumin over 12 h.

Furthermore, the release rate of curcumin fits best to the first-order kinetic model ($R^2 = 0.983$, $K1 = 0.000982 \text{ min}^{-1}$), suggesting concentration-dependent release. While the second-order kinetic model also described the release profile adequately, it was observed that the second-order fit ($R^2 = 0.981$, $K2 = 0.151258 \text{ min}^{-1}$) was slightly lower (Fig. 11). These results indicate that the drug release rate is predominantly concentration-dependent, consistent with first-order kinetics governing the release process. Thus, the study of release kinetics complements the mechanistic insights obtained from the Korsmeyer–Peppas model by confirming that the drug release follows first-order kinetics, rather than solely mechanistic interpretations.

Antibacterial activity

The Kirby–Bauer disk diffusion test was employed to test the antibacterial activity of the native GG and curcumin-loaded

EGG (EGG-cur) film. Fig. 12a–e shows the susceptibility of GG and EGG cur against *E. coli* and *S. aureus* Gram-negative and Gram-positive strains, respectively. As assumed, the native GG film did not exhibit any antibacterial activity, whereas the EGG-cur film showed significant antibacterial activity. Distinct inhibition zones of $23 \pm (0.01) \text{ mm}$ and $18 \pm (0.01) \text{ mm}$, respectively, are observed around the curcumin-loaded EGG films against these bacterial strains. This is primarily because of the strong antimicrobial action of curcumin, which has been synergistically enhanced by the crosslinked EDTA in the EGG films.

Antifungal activity

The antifungal activity was performed against the *A. niger* fungal species. As shown in Fig. 12c, the native GG showed no fungal prohibition around its periphery. However, considerable retardation in fungal growth around the EGG films periphery is observed, which is depicted in Fig. 12e. Hence, the Kirby–Bauer disk diffusion test demonstrated that the curcumin-loaded crosslinked EGG film exhibited pronounced antifungal activity by retarding the fungal growth of *A. niger* around the periphery of the EGG films.

Antioxidant activity

The antioxidant activity of GG and modified GG with different concentrations of EDTA, along with curcumin impregnation, was measured using DPPH radical scavenging activity, and the results are displayed in Fig. 13. It is observed that the initial $48.3 \pm (0.13)\%$ of antioxidant activity is mainly due to native GG. The antioxidant potential increases as the crosslinking concentration of EDTA increases from 0.25 g to 1 g, and shows an increment from $68.4 \pm (0.2)\%$ to $90.8 \pm (0.5)\%$. However, it is also observed that the curcumin-impregnated EGG film showed a maximum antioxidant potential of $94.3 \pm (0.5)\%$. This is probably because of the synergistic impact of both EDTA and curcumin towards enhancing the antioxidant properties of the EGG films.

Experimental section

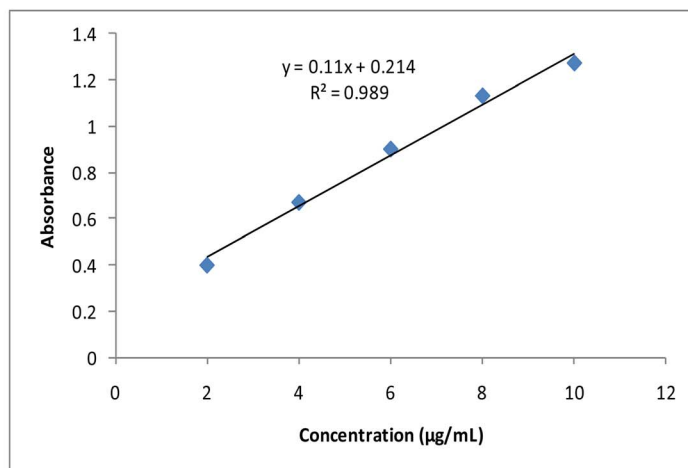
Material and methods

Guar gum (GG; M/G ratio = 1.8 : 1; molecular weight = 2 10 000 Da; viscosity = 5800 cps (1%, 25 °C)) was procured from M/s Sunita Hydrocolloids Pvt., Ltd, Jodhpur. Ethylene-diaminetetraacetic acid (EDTA) and curcumin of laboratory grade were purchased from SRL Chemicals, Mumbai, India. Monopotassium phosphate (KH_2PO_4), dipotassium phosphate (K_2HPO_4) and 2,2-diphenyl-1-picrylhydrazyl (DPPH) were purchased from SD Fine-Chem Limited, Mumbai, India. Nutrient agar medium (NAM) and potato dextrose agar (PDA) were purchased from HiMedia, Mumbai, India.

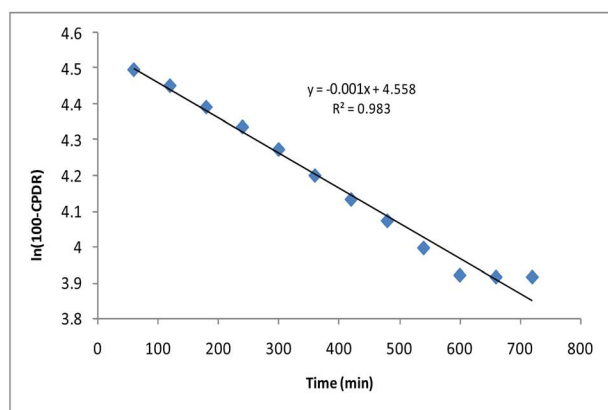
Table 3 Curcumin release profile and loading efficiency of EGG

Sample	Model	R^2	n	k	Release mechanism	DLC%	EE%
EGG	Korsmeyer–Peppas	0.9987	0.76	0.37	DCR	$7.92 \pm (0.2)$	$72.2 \pm (0.5)$

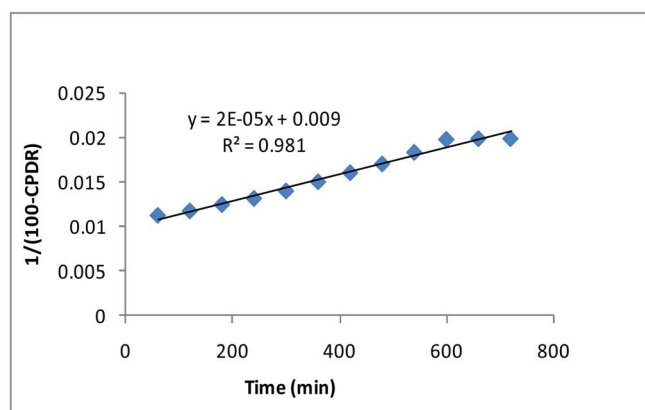




(a)



(b)



(c)

Fig. 11 (a) Standard curve of curcumin. (b) First-order release kinetic profile plot of $\ln(100\text{-CPDR})$ against time (min). (c) Second-order release kinetic profile plot of $1/(100\text{-CPDR})$ against time (min).

Preparation of EDTA-crosslinked guar gum (EGG) films

A homogeneous 1% (w/v) aqueous solution of GG was prepared by dissolving 1.0 g of GG in 100 mL of distilled water, and stirred at 500 rpm for 1 h to attain maximum viscosity. Concurrently, the EDTA solution (0.25, 0.5, 0.75 and 1.0 g in 10 mL in distilled water) was adjusted to pH 6.2 by 1 M NaOH. Each EDTA solution (10 mL) was introduced dropwise using a micropipette to the homogeneous viscous solution of GG under constant stirring at 55 °C for another 1 h, with the pH 5.0 maintained by dropwise addition of 1 N HCl during the reaction. After completion, the reaction mixture was adjusted to pH 7.0, degassed, cast onto a Teflon plate at room temperature for 30 min, and oven dried at 55 °C for 48 h. The resulting films were thermally cured at 120 °C, 130 °C and 140 °C for 3, 2, and 1 min, respectively, to obtain the crosslinked EGG films with optimized morphology. Finally, the films were peeled from the plate, washed thoroughly with deionized water, and stored in polyethylene bags for subsequent characterization. The

crosslinking films cured at different curing temperatures are shown in Fig. 14.

Quantification by the degree of diesterification

The degree of diesterification has been calculated using complexometric titration, taking a cue from the previous study of Menzel *et al.*, 2013.³⁴ Briefly, two solutions were titrated against 0.02 M CuSO_4 solution. In the first titration, 200 mg weighed EDTA-crosslinked guar gum film (EGG) was hydrolyzed in 25 mL (0.1 M) KOH solution for 20 min. This gives the total amount of EDTA consumed in the film. In the second titration, 200 mg weighed EGG was immersed in distilled water (25 mL). This will give the total content of free EDTA and monoesters present in the EGG film. As an indicator, murexide was introduced into the solution of 0.02 M CuSO_4 , which displayed an orange color, and indicated a light pink color at the endpoint. The total EDTA diester content was calculated as follows:

$$\text{Total EDTA diester } (W_{\text{di-ester}}) = \text{total EDTA content present in the film} - (\text{free EDTA} + \text{monoester of EDTA})$$



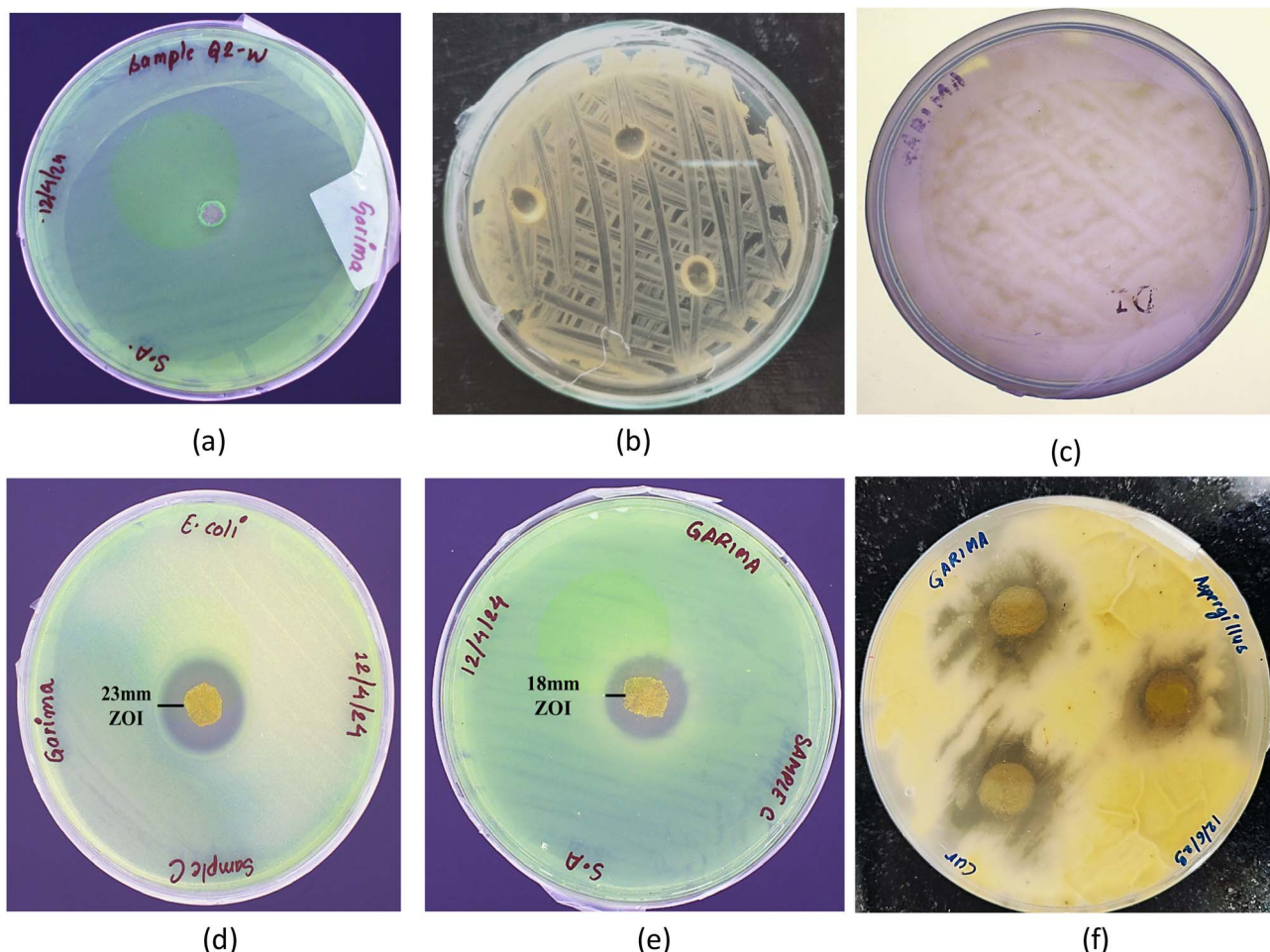


Fig. 12 (a) Antibacterial activity of GG against *S. aureus*. (b) Antibacterial activity of GG against *E. coli*. (c) Antifungal activity of GG against *A. niger*. (d) Antibacterial activity of EGG against *E. coli* with a 23-mm zone of inhibition (ZOI). (e) Antibacterial activity of EGG against *S. aureus* with a 18-mm zone of inhibition (ZOI). (f) Antifungal activity of EGG against *A. niger*.

The degree of diesterification (D.D.E) was calculated as follows:

$$\text{D.D.E} = 2 \times \frac{M_{\text{ma}} \times W_{\text{di-ester}} \times M_{\text{AGU}}}{M_{\text{Ma}} \times M_{\text{gg}}}$$

where M_{ma} is the weight of EDTA used, $W_{\text{di-ester}}$ is the weight of di-ester calculated, M_{AGU} is the mass per anhydroglucose unit of GG, M_{Ma} is the molecular weight of EDTA, and M_{gg} is the molecular weight of GG.

Swelling behavior and solubility

To study the swelling behavior and solubility, 200 mg of EGG film was dissolved in 10 mL of distilled water and stored for 24 h. Afterwards, samples were heated over a water bath at 85 ± 2 °C for 10 min, followed by centrifugation at 3000 rpm for 10 min.³⁹ The swelling test was performed as follows:

$$\text{Swelling behavior(\%)} = \frac{W_1 - W_0}{W_0} \times 100$$

where W_1 is the weight of the swollen film, and W_0 is the weight of the initially taken dry film sample.

To examine the solubility of EGG, the supernatant was taken in a Petri dish and dried at 70 ± 2 °C for 24 h in an oven, and afterwards formulated as given below:

$$\text{Solubility(\%)} = \frac{W_e - W_f}{W_f} \times 100$$

where W_e is the weight of the Petri dish dried for 24 h and W_f is the initial weight of the Petri dish.

3.5 Characterization of GG and EGG films

The detailed characterizations were systematically performed. The FTIR spectra of samples GG and EGG were recorded through a Cary 630 FT-IR spectrometer (Agilent Technologies, USA) with a resolution of 4 cm^{-1} in the wavenumber range of $400\text{--}4000 \text{ cm}^{-1}$. The crystallinity of the samples was examined using the X-ray diffraction (XRD) method on a Rigaku Smart Lab X-ray diffractometer with detector D/tEX Ultra 250 and filter 1D Cu K α radiation. The scan speed was $2 \text{ }^\circ\text{C min}^{-1}$ for Bragg's angle (2θ), which is in the 50–800 nm range. For the investigation, the device was set to 40 kV and 50 mA. The surface morphology of GG and EGG was studied *via* scanning electron microscopy (SEM) and SEM-EDX, respectively, using the SEM-



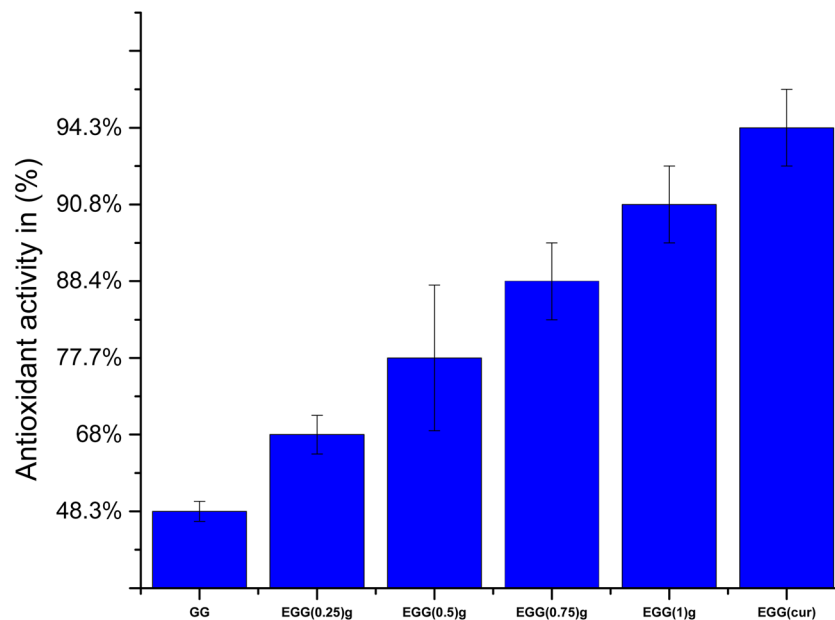


Fig. 13 Antioxidant activity of the GG and EGG films at different concentrations of EDTA.

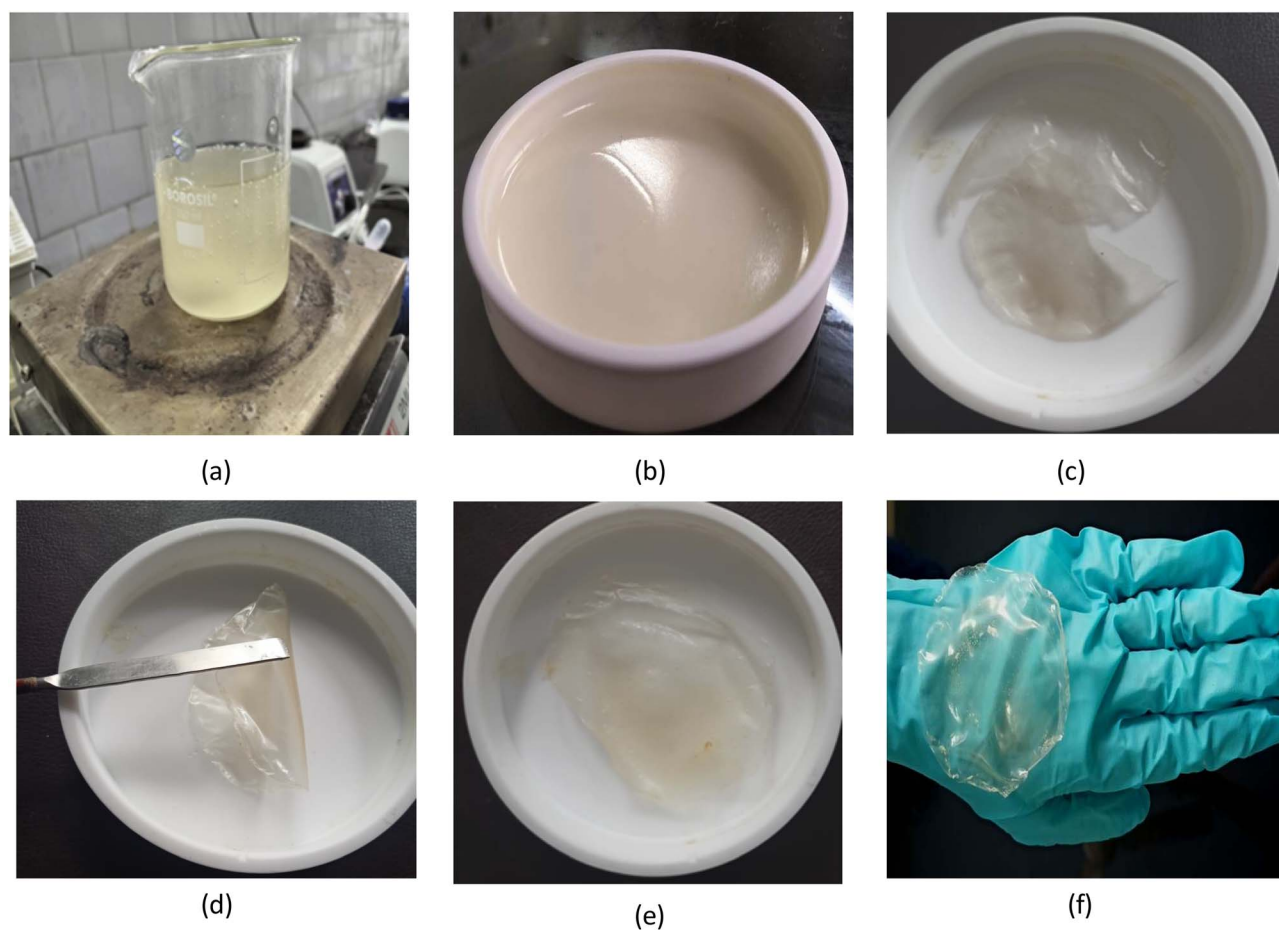


Fig. 14 (a) Viscous crosslinked solution formed after 1 h of reaction. (b) Degassed crosslinked solution casted on a Petri plate. (c) Crosslinked EGG film cured at 120 ± 1 °C with a fractured surface. (d) Crosslinked EGG film cured at 130 ± 1 °C with a flexible and smooth morphology. (e) Crosslinked EGG film cured at 140 ± 1 °C with a slight brown texture and rough morphology. (f) Crosslinked film cured at 130 ± 1 °C with a suitable morphology for serving as the TDDS.



Carl Zeiss EV018 instrument. Their thermal stability and degradation behavior were investigated using a thermogravimetric analyzer (Discovery TGA55, TA instruments) in a nitrogen environment at a rate of $5 \pm 1 \text{ }^\circ\text{C min}^{-1}$. Samples were investigated under the temperature range between $25 \pm 1 \text{ }^\circ\text{C}$ to $800 \pm 1 \text{ }^\circ\text{C}$. A digital micrometer was used to measure the thickness of all films.⁴⁰ The universal testing machine (UTM) (Tinius Olsen Limited, UK, Model-25ST) was used with a gauge length of 25 mm and a crosshead speed of 50 mm min^{-1} . The standard deviation and mean thickness were calculated. The mechanical properties of the rectangular pieces of samples GG and EGG with dimensions of about $5 \text{ cm} \times 1 \text{ cm}$ were measured under humid conditions of $55 \pm 0.3\%$ while maintaining a temperature of $27 \pm 2 \text{ }^\circ\text{C}$, according to ASTM D882-02. For the recording of liquid state NMR, a Bruker AV 500 MHz spectrometer was used. The samples GG and EGG were hydrolyzed for 4 h with 1 M HCl, followed by co-distillation with methanol over a rotatory evaporator. After drying, samples were lyophilized at $-60 \pm 2 \text{ }^\circ\text{C}$ and deuterium exchange was done 3–4 times. Furthermore, samples were filtered through a $0.45 \text{ }\mu\text{m}$ syringe filter, collected in an Eppendorf tube and weighed. For the ^1H NMR spectrum at 500.17 MHz, 512 scans were recorded with 2.2282 s data acquisition time for the FID, having a relaxation delay of 1 s. For the ^{13}C NMR at 125.78 MHz, 2048 scans were recorded.

Curcumin loading and *in vitro* release study

Curcumin loading. Curcumin has been chosen as a ‘model drug’ to study its release profile from the EGG film matrix. After developing the crosslinked EGG film, the cured EGG film ($130 \pm 1 \text{ }^\circ\text{C}$ for 2 min) was dipped in 100 ppm of ethanolic solution of curcumin for 24 h.^{33,41} In due course, the prepared curcumin-loaded EGG film was washed thoroughly with ethanol to remove any portions of unloaded curcumin.

Curcumin loading and encapsulation efficiency

To investigate the loading potential of the EGG matrix, 500 mg of the curcumin-loaded EGG film was completely disrupted in 50 mL of acetone and constantly stirred for 48 h to extract the loaded curcumin from the film. The solution was filtered and assayed by a UV spectrophotometer at 491.2 nm as performed in our previous work.³³ The percentage content of drug loading capacity (DLC) and drug encapsulation efficiency (DEE) was calculated as follows:⁴²

$$\text{DLC \%} = \frac{\text{entrapped drug}}{\text{weight of drug} - \text{drug loaded film}} \times 100$$

$$\text{DEE \%} = \frac{\text{drug added} - \text{free drug}}{\text{drug added}} \times 100$$

In vitro curcumin release

To examine the efficacious transdermal release of curcumin from the EGG film, 200 mg of film was placed in a measured

volume (50 mL) of phosphate buffer saline (PBS) solution with pH 7.4 at $37 \pm 2 \text{ }^\circ\text{C}$.⁴³ This is because chronic wounds and infectious skin sites have an alkaline environment with the pH value ranging from 7–9. The amount of curcumin release was determined at different time intervals by measuring the absorbance of the release medium with a UV-vis spectrophotometer at 491.2 nm. The calibration graph was plotted to obtain the correlation coefficient (R^2) value. Subsequently, the cumulative percentage drug release (CPDR) of curcumin was calculated.^{43,44}

Kinetic study of curcumin release

The kinetics of curcumin release data were analyzed using mathematical modeling. The cumulative percentage drug release (CPDR) data were studied against time, and the amount of curcumin that was released at regular time intervals was fitted into the different models. For interpretation of the mechanism, the Korsmeyer–Peppas model has been used.⁴⁵ Additionally, to quantitatively assess the kinetics of curcumin release, both first-order and second-order kinetic models were applied to the release data.⁴⁸ The first-order kinetics model assumes that the release rate of the drug depends on the amount of drug remaining in the matrix, while the second-order kinetics model considers that the release rate depends on the square of the amount of drug remaining. Eqn (1)–(3) used in the different model studies are discussed below:

$$\text{Korsmeyer–Peppas model: } M_t/M_{\text{eq}} = k \times t^n \quad (1)$$

where M_t is the amount of drug released at time t , M_{eq} is the total amount of drug in dosage form, and k and n are the kinetic constant and release exponent, respectively. If the value of n is below 0.5, it denotes Fickian diffusion. If the value of n lies between 0.5 and 1, it depicts an anomalous or non-Fickian transport.

First-order kinetics:

$$F = 1 - e^{-(k_1 \times t)} \quad (2)$$

where F is the fraction of percentage of curcumin release, k_1 is the first-order release rate constant and t is the time period of drug release.

Second-order kinetics:

$$t/M_t = 1/k_2 \times M_{\text{equilibrium}}^2 + (1/M_{\text{equilibrium}}) \times t \quad (3)$$

where M_t is the amount of drug released at time (t), $M_{\text{equilibrium}}$ is the total amount that can be released at 100% and k_2 is the second-order rate constant.

Antibacterial activity of curcumin-loaded films

The bacteria used in this study were *E. coli* and *S. aureus*, Gram-negative and Gram-positive strains, respectively. These strains were procured from the Health Sciences Division, UPES, Dehradun, India. The cultures were maintained at $4 \pm 2 \text{ }^\circ\text{C}$ on a nutrient broth (NB). The active cultures of strains for experiments were prepared by transmitting a loop full of cells from Petri plates to test tubes of nutrient broth, which were then



incubated for 24 h at 37 ± 2 °C. Nutrient broth medium (NAM) was used for further susceptibility testing. To study the antibacterial activity, the Kirby–Bauer method (also known as the disk diffusion method) was employed.³⁹ Culture plates were prepared by pouring 20 mL of sterile nutrient agar medium, and each inoculum suspension was swabbed onto the agar surface. Discs of samples GG and EGG were placed, and culture plates were incubated for 24 h at 37 ± 2 °C. The further activity was calculated by measuring the diameter of zone of inhibition with the help of a scale (mm).

Antifungal activity of curcumin-loaded films

The fungus strain used for the study was *A. niger*. This strain was procured from the Health Sciences Division, UPES, Dehradun, India. The culture was prepared in PDA slant at 4 ± 2 °C. For experimentation, the fungal strain was revived and subcultured on PDA plates, which were incubated at 29 ± 2 °C for 48 h.

To study the antifungal activity, the Kirby–Bauer method was performed. After pouring 20 mL of PDA, culture plates were prepared. Each spore suspension was swabbed onto the media plates, which were then incubated at 29 ± 2 °C for 3–4 days. Afterwards, the fungal growth was examined.

Antioxidant activity

The antioxidant activity of native GG and EGG films at different concentrations of EDTA and curcumin-loaded EGG films was evaluated using 2,2-diphenyl-1-picrylhydrazyl radical (DPPH). Initially, a 50 mL methanolic solution of 0.1 mM DPPH was prepared. Small squares of the sample (20×20 mm) were cut and dipped in 10 mL DPPH methanolic solution, and incubated at room temperature for 30 min in dark conditions. After incubation, the absorbance at 517 nm was measured using a UV-Vis spectrophotometer.⁴⁷ The formula used is given below:⁴⁸

$$\% \text{Scavenging} = [(\text{Abs. blank} - \text{Abs. sample}) / \text{Abs. blank}] \times 100$$

where Abs.blank is the absorbance of the blank (DPPH + methanol) and Abs.sample is the absorbance of the film sample (DPPH + methanol + film).

Statistical analysis

For each investigation, the swelling, solubility, antioxidant, thickness, and mechanical properties were measured in triplicate. Statistical analysis was done using one-way ANNOVA. 0.05 was taken as the level of significance. The centrality level of $P < 0.05$ was used.

Conclusions

The present study has been planned by thoughtful curation of the reaction design, keeping green chemistry principles at the forefront. A key principle is the selection of safe, eco-friendly reagents, namely the abundant agricultural biopolymer guar galactomannan and EDTA, a non-toxic, cost-effective, self-catalyzing crosslinker. By substituting EDTA for traditional

toxic crosslinkers, we achieved efficient crosslinking under catalyst-free conditions and with a streamlined workup. The degree of diesterification ranged from $0.0077 \pm (1.0 \times 10^{-4})$ to $0.0295 \pm (1.5 \times 10^{-4})$. Crosslinking decreased swelling and simultaneously increased solubility. EGG films were characterized by SEM-EDX, confirming a porous network and elemental composition. FTIR revealed an ester band at 1735 cm^{-1} . High-resolution $^1\text{H}/^{13}\text{C}$ NMR, HSQC, and HMBC spectra further corroborated the ester linkage formation. XRD revealed increased semi-crystallinity, while TGA demonstrated improved thermal stability with three distinct degradation stages. Curcumin-loaded EGG exhibited non-Fickian release over 720 min, and pronounced antibacterial, antifungal, and anti-oxidant activities. These findings underscore the feasibility of converting renewable biomass into advanced biomaterials, reducing dependence on non-renewable and non-biodegradable resources, and extending EDTA's utility beyond chelation to sustainable material applications.

Author contributions

J. R.: investigation, methodology, writing – original draft. V. K.: conceptualization, data curation, funding acquisition, project administration, resources, supervision, validation, visualization, writing – review & editing. K. C.: supervision, visualization. D. K.: resources, supervision. G. S.: resources, methodology. A. M.: resources.

Conflicts of interest

The authors declare no conflict of interest.

Data availability

The authors confirm that the data supporting the findings of this study are available within the article and supplementary information (SI). Supplementary information: the tables demonstrating the degree of diesterification, solubility, and swelling behavior are given. The SEM morphology and TGA graph of the native GG, and the 1D and 2D NMR spectra of GG and EGG are provided. The figure for the CPDR% drug release is also given, along with the graphs of activation energy calculations for the GG and EGG crosslinked films. See DOI: <https://doi.org/10.1039/d5su00309a>.

Acknowledgements

The authors express their sincere appreciation to the Director, Forest Research Institute (ICFRE), Dehradun, India, for providing laboratory facilities. One of the authors is thankful to the Central University of Haryana, Mahendragarh, India, for providing the CUCET fellowship. The authors are also grateful to the Sophisticated Analytical Instrumental Facility (SAIF), Panjab University, Chandigarh, for recording the spectral data, Uttaranchal University, Dehradun, for SEM and XRD studies and Central Institute of Petrochemicals Engineering & Technology (CIPET), Dehradun, for TGA and tensile studies.



References

- W. Schlemmer, J. Selinger, M. A. Hobisch and S. Spirk, *Carbohydr. Polym.*, 2021, **265**, 118063.
- M. Luo, X. Zhang, J. Wu and J. Zhao, *Carbohydr. Polym.*, 2021, **266**, 118097.
- L. Xie, M. Shen, Y. Hong, H. Ye, L. Huang and J. Xie, *Carbohydr. Polym.*, 2020, **229**, 115436.
- X. Chen, M. Shen, Q. Yu, Y. Chen and J. Xie, *Trends Food Sci. Technol.*, 2024, **144**, 104317.
- J. Maitra and V. K. Shukla, *J. Polym. Sci.*, 2014, **4**, 25–31.
- D. Duquette and M. J. Dumont, *Polym. Bull.*, 2019, **76**, 2683–2710.
- E. Orzan, A. Barrio, V. Biegler, J. B. Schaubeder, A. Bismarck, S. Spirk and T. Nypelö, *Carbohydr. Polym.*, 2025, **347**, 122617.
- A. K. Sonker, K. Rathore, A. K. Teotia, A. Kumar and V. Verma, *J. Appl. Polym. Sci.*, 2019, **136**, 47393.
- N. Schafer, R. Balwierz, P. Biernat, W. Ochędzan-Siodłak and J. Lipok, *Mol. Pharm.*, 2023, **20**, 3278–3297.
- M. R. Saboktakin, S. Akhyari and F. A. Nasirov, *Int. J. Biol. Macromol.*, 2014, **69**, 442–446.
- M. Mahinroosta, Z. J. Farsangi, A. Allahverdi and Z. Shakoori, *Mater. Today Chem.*, 2018, **8**, 42–55.
- L. Z. Wang, L. Liu, J. Holmes, J. F. Kerry and J. P. Kerry, *Int. J. Front. Sci. Technol.*, 2007, **42**, 1128–1138.
- J. Chrobak, J. Iłowska and A. Chrobok, *Molecules*, 2022, **27**, 4862.
- M. A. Collins, *Appl. Occup. Environ. Hyg.*, 2002, **17**, 846–855.
- W. H. Lawrence, M. Malik, J. E. Turner and J. Autian, *J. Pharm. Sci.*, 1972, **61**, 1712–1717.
- R. O. Beauchamp, M. B. G. St Clair, T. R. Fennell, D. O. Clarke, K. T. Morgan and F. W. Karl, *Crit. Rev. Toxicol.*, 1992, **22**, 143–174.
- J. M. Carvajal-Arroyo, P. Candry, S. J. Andersen, R. Props, T. Seviour and R. G. K. Rabaey, *Green Chem.*, 2019, **21**, 1330–1339.
- C. Zhuang, F. Tao and Y. Cui, *RSC Adv.*, 2015, **5**, 52183–52193.
- A. Pangon, S. Saesoo, N. Saengkrit, U. Ruktanonchai and V. Intasanta, *Carbohydr. Polym.*, 2016, **138**, 156–165.
- N. Murali, K. Srinivas and B. K. Ahring, *Ferment.*, 2017, **3**, 22.
- M. Llamas, S. Greses, E. Tomás-Pejó and C. González-Fernández, *Bioresour. Technol.*, 2022, **344**, 126282.
- Y. J. Zhou, P. Luner and P. Caluwe, *J. Appl. Polym. Sci.*, 1995, **58**, 1523–1534.
- L. Gautam, S. G. Warkar, S. I. Ahmad, R. Kant and M. Jain, *Poly. Eng. Sci.*, 2022, **62**, 225–246.
- C. Q. Yang, *J. Polym. Sci. Part A: Polym. Chem.*, 1993, **31**, 1187–1193.
- T. G. Dastidar and A. N. Netravali, *Carbohydr. Polym.*, 2012, **90**, 1620–1628.
- T. Harifi and M. Montazer, *Carbohydr. Polym.*, 2012, **88**, 1125–1140.
- S. Zakaria, The Study of Wet-Strength Development by Di and Polycarboxylic Acids and Anhydrides, PhD Thesis, The University of Manchester, United Kingdom, 1994.
- C. E. Noradounand and I. F. Cheng, *Environ. Sci. Technol.*, 2005, **39**, 7158–7163.
- T. R. Thomsen, L. Hall-Stoodley, C. Moser and P. Toodley, *Biofilm Infections*, 2011, 91–109.
- R. J. W. Lambert, G. W. Hanlon and S. P. Denyer, *J. Appl. Microbiol.*, 2004, **96**, 244–253.
- A. Cay and M. Mirafteb, *J. Appl. Polym. Sci.*, 2013, **129**, 3140–3149.
- Y. H. Yun, Y. J. Wee, H. S. Byun and S. D. Yoon, *J. Polym. Environ.*, 2008, **16**, 12–18.
- J. Rajput, V. Kumar, K. Chauhan, V. Parkash and S. Bhattarai, *Green Chem.*, 2024, **26**, 5417–5432.
- C. Menzel, E. Olsson, T. S. Plivelic, R. Andersson, C. Johansson, R. Kuktaite and K. Koch, *Carbohydr. Polym.*, 2013, **96**, 270–276.
- D. Dangi, M. Mattoo, V. Kumar and P. Sharma, *Carbohydr. Polym. Technol. Appl.*, 2022, **4**, 100230.
- E. Akar, A. Altınışık and Y. Seki, *Carbohydr. Polym.*, 2012, **90**, 1634–1641.
- D. Dangi, P. Sharma and V. Kumar, *J. Appl. Polym. Sci.*, 2022, **139**, 51669.
- H. Kono, F. Otaka and M. Ozaki, *Carbohydr. Polym.*, 2014, **111**, 830–840.
- J. J. Biemer, *Ann. Clin. Lab. Sci.*, 1973, **3**, 135–140.
- M. S. Rao, S. R. Kanatt, S. P. Chawla and A. Sharma, *Carbohydr. Polym.*, 2010, **82**, 1243–1247.
- K. K. Majumder, J. B. Sharma, M. Kumar, S. Bhatt and V. Saini, *Pharmacophore*, 2020, **11**, 115–121.
- D. Dangi, M. Mattoo, V. Kumar and P. Sharma, *Carbohydr. Polym. Technol. Appl.*, 2022, **4**, 100230.
- K. Vimala, M. M. Yallapu, K. Varaprasad, N. N. Reddy, S. Ravindra, N. S. Naidu and K. M. Raju, *J. Biomater. Nanobiotechnol.*, 2011, **2**, 55.
- R. Patel, S. K. Singh, S. Singh, N. R. Sheth and R. Gendle, *Int. J. Pharm. Sci. Res.*, 2009, **1**, 71.
- A. Bajpai and V. Raj, *Polym. Bull.*, 2021, **78**, 4109–4128.
- A. Agrawal and R. Purwar, *Indian J. Fibre Text. Res.*, 2018, **43**, 104–111.
- D. Arrua, M. C. Strumia and M. A. Nazareno, *J. Agric. Food Chem.*, 2010, **58**, 9228–9234.
- T. Thanyacharoen, P. Chuysinuan, S. Techasakul, P. Noeaid and S. Ummartyotin, *Int. J. Biol. Macromol.*, 2018, **107**, 363–370.
- W. Ma, H. Lu, Y. Xiao and C. Wu, *Organ. Res.*, 2025, **1**, 025040004.
- S. W. A. Shah, X. Li, H. Yuan, H. Shen, H. S. Quan, G. Pan and J. Shao, *BMEMat*, 2025, e70001.
- S. Maiti, B. Maji and H. Yadav, *Carbohydr. Polym.*, 2024, **326**, 121584.
- C. Wang, Y. Wang, X. Lan, L. Zhu, J. Gu, W. Hou and W. Xu, *ACS Mater. Lett.*, 2025, **7**, 1795–1806.
- S. A. Atanda, R. O. Shaibu and F. O. Agunbiade, *J. Mater. Sci.*, 2024, **19**, 22.
- S. Elkatatny, M. Mahmoud and K. Abdelgawad, *Arabian J. Sci. Eng.*, 2018, **43**, 6481–6491.

